Microelectronics Reliability 53 (2013) 41–46

Contents lists available at SciVerse ScienceDirect

Microelectronics Reliability

journal homepage: www.elsevier.com/locate/microrel

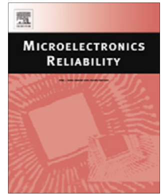

Analysis of bump resistance and current distribution of ultra-fine-pitch microbumps

Y.W. Chang [a], H.Y. Peng [a], R.W. Yang [a], Chih Chen [a,*], T.C. Chang [b], C.J. Zhan [b], J.Y. Juang [b], Annie T. Huang [c]

[a] *Department of Materials Science and Engineering, National Chiao Tung University, Hsin-chu 30010, Taiwan, ROC*

[b] *Introduction of Electronics & Optoelectronics Research Laboratories, Industrial Technology Research Institute, Hsin-chu, 31040 Taiwan, ROC*

[c] *Research Center for Applied Sciences, Academia Sinica, Taipei, 11529 Taiwan, ROC*

ARTICLE INFO

Article history:
Received 16 December 2011
Received in revised form 24 August 2012
Accepted 24 August 2012
Available online 26 September 2012

ABSTRACT

To keep up with the demand of continuous increase in device densities, the integration of three-dimensional integrated circuits (3D-IC) has become the most probable solution, and the utilization of ultra-fine-pitch microbump has emerged as an essential component of 3D-IC technology. In this study, a Kelvin bump structure was fabricated and resistances measured at different angles on a 20.0 μm microbump were investigated. The microbump resistance at 0°, 60°, 120°, and 180° are 74.7, 45.9, 14.6, and 13.7 mΩ, respectively. These high resistances in microbumps may result in high interconnect resistance and cause resistance/capacitance (RC) delay, and thus lower the electrical performance of 3D-IC. A series of finite-element-model (FEM) was built to analyze the distribution of electric field in microbump. The FEM results have shown that the current is distributed uniformly in the thin solder joint, but current crowding still occurs in the Cu under-bump-metallization (UBM). The finding of the current crowding in the Cu UBM is the main cause of high resistances in the microbump. Thickening the Al trace, for example, from 0.4 μm to 1.5 μm, is a direct solution to reduce the unexpected high microbump resistance. A numerical model which treated solder joints as a resistance network was also performed in this study. For comparison, both FEM and the numerical model show the same trend and agree with the measurement results from Kelvin bump structure. The results all point to one thing: thickening the Al trace turn out to be the most effective approach to reduce high microbump resistance. When the Al trace thickness is increased from 0.8 to 3.0 μm, the microbump resistance is decreased to half of the original value, resulted from the alleviation of current crowding in the Cu UBM.

© 2012 Elsevier Ltd. All rights reserved.

1. Introduction

In order to keep up with the increasing demand of higher density and Input/Output (I/O) number for high performance electronics, size of individual devices must shrink accordingly. However, further shrinking of device size under nano-scale is extremely challenging and not cost effective. Consequently, some solutions had been proposed to maintain the inevitable trend and three-dimensional integrated circuit (3D-IC) has emerged as a preferable solution for the next-generation products. 3D-IC can be utilized is mostly due to the improvement of three key technologies: wafer thinning, through-silicon-via fabrication, and microbump bonding whereas microbumps play an important role that serve as interconnects between different chips [1–3]. Presently, 3D-IC is mostly fabricated by stacking chips vertically and interconnecting chips with wire-bonding at the edge of chips. Such packaging method reduces the product size, but the electrical performance is limited by the high resistance and the inductance of the wires. Significant resistance/capacitance (RC) delay may occur when the resistance of the wire is large. Therefore, the utilization of ultra-fine-pitch microbump has become the most promising alternative to replace the wire-bonding in 3D-IC due to its shorter interconnection and higher density.

The main difference between a microbump and a flip-chip bump is the dimension and the volume, which significantly affect both electrical performance and metallurgical reactions. The dimensions of flip-chip bumps are usually 100 μm in diameter and 100 μm in height. However, the diameter and the height of a microbump are about 20–30 μm, which is only one fifth of a flip-chip bump. As a result, the contact area of a microbump is only 4% of a flip-chip bump, and the volume is less than 1% of a flip chip bump. The reduction of dimensions and the volume dramatically affect the electrical performance and metallurgical reactions. In today's circuit design, each solder joint will carry 0.2 A and it is expected to be doubled in the near future [4]. As a result, the average current density in a 20-μm diameter microbump is about 5×10^4 A/cm^2 when a current of 0.2 A is applied. Electromigration effect in the solder is activated under this kind of high current density [5–7]. Therefore, it is an urgent issue to understand the

* Corresponding author.
E-mail address: chih@mail.nctu.edu.tw (C. Chen).

0026-2714/$ - see front matter © 2012 Elsevier Ltd. All rights reserved.
http://dx.doi.org/10.1016/j.microrel.2012.08.021

electrical behavior inside a single ultra-fine-pitch microbump solder joint. Some researchers have reported the value of resistances in microbumps, but there is no reported study specifically discussing the current density distribution, and the relationship between the current crowding effect and the microbump resistance [8–12]. In this study, Kelvin bump structures (KBSs) with different measured angles were designed and fabricated. After measuring the bump resistance of a single microbump at different angles, we found that the resistance of a microbump approached 75 mΩ [13–15]. Previous studies mentioned that the bump resistance of a flip-chip solder joint is only several milliohms. The one-order higher bump resistance of the microbump brings about serious RC delay. Furthermore, the resistive microbump produces considerable Joule heating, which is quite different from traditional flip-chip solder joints. To further understand the phenomena, a series of three dimensional finite element models (3D-FEM) was performed in this study to explain the cause of the high microbump resistance and to reveal the electrical behavior inside the microbump. Furthermore, the 3D-FEM results provide a most effective solution to reduce high microbump resistance, that is "thickening the Al traces". Finally, a simplified numerical model was created to explain the relationship between the electrical distribution and the bump resistance.

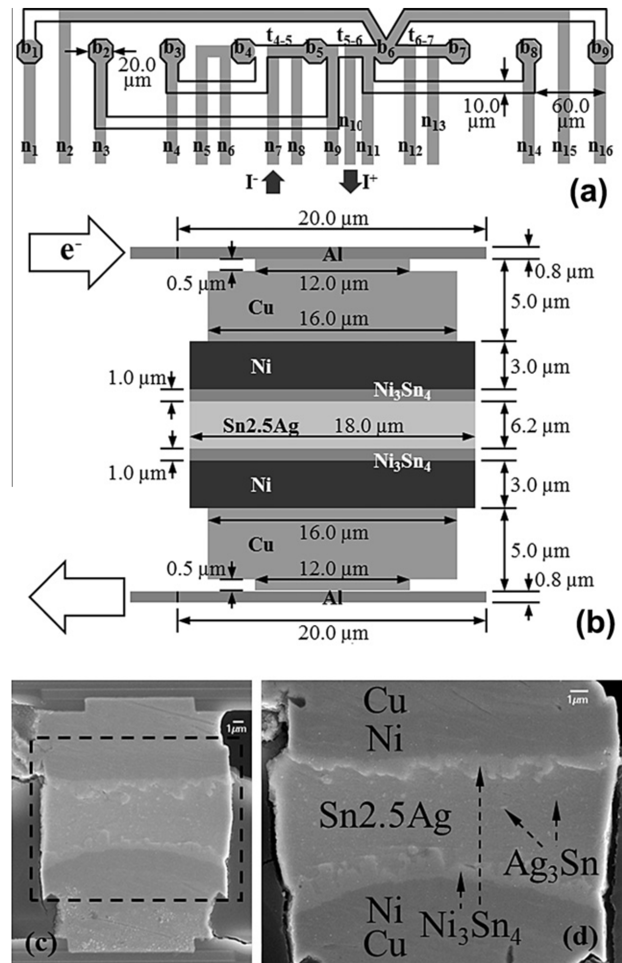

Fig. 1. (a) Plan view of Kelvin bump structures. (b) Cross-sectional schematic of a microbump. (c) Cross-sectional SEM image of a microbump. (d) The enlarged image of the dotted square in (c).

2. Experimental procedure

2.1. Kelvin bump structures and measurement

A KBS was successfully fabricated to precisely measure the bump resistance of a single microbump in this study. The schematic plots and the cross-sectional scanning electron microscope (SEM) images are shown in Fig. 1. Due to the requirement of high alignment accuracy, chip-to-chip (COC) method was applied. The thicknesses of chips on both die-side and substrate-side are 760.0 µm and the Al traces on both sides of chips are 0.8 µm thick and 10.0 µm wide. Fig. 1a is the plan-view layout of a KBS. Solid lines represent the layout of die-side Al traces, and gray-color regions represent the layout of substrate-side traces. In this structure, 16 nodes are marked as n_1, n_2 ... n_{16}, and nine microbumps are marked as b_1, b_2 ... b_9. The pitch of these bumps is 60.0 µm. There are also 3 die-side traces constructing a direct link between b_4 and b_7 and marked as $t_{4–5}$, $t_{5–6}$, and $t_{6–7}$. With this KBS, the bump resistance at different angles of b_5 and b_6 can be in situ monitored during various kinds of reliability tests.

As shown in Fig. 1a, a 0.02 A current was applied through n_7 and n_{10} at 100 °C. In other words, the electricity flows through n_7, b_5, $t_{5–6}$, b_6, and n_{10}. The direction of electron flow is upward in b_5 and downward in b_6. The methods of microbump resistance measurement at different angles of b_5 and b_6 are listed in Table 1. We monitor 7 microbump resistances simultaneously in this study (two in b_5, four in b_6, and one in $t_{5–6}$). Each resistance was monitored every 20 s for a total of 10 min and then the values are averaged to eliminate the influence of temperature fluctuation.

The schematic plot of cross-sectional microbump image is shown in Fig. 1b, and the bump structure is longitudinally symmetric. The thickness of electroplated Cu/Ni under bump metallization (UBM) is 5.0/3.0 µm. The diameter of the Al pad, passivation opening, and UBM opening are 20.0 µm, 12.0 µm, and 18.0 µm respectively. As shown in Fig. 1c and d, the thickness of the inter-metallic compound (IMC) is about 1 µm at the interface of the Ni UBM and the Sn2.5Ag solder is about 1.0 µm thick. The height of the remaining Sn2.5Ag solder is only 6.2 µm and there are some precipitated nanometer-sized Ag_3Sn particles uniformly dispersed in the β–Sn matrix. The dimensions and the compositions were obtained by SEM and EDS.

Table 1
The experimental setup for the measurement nodes of microbump resistances for b_5, $t_{5–6}$, and b_6. The resistance of b_5 can be measured either from 0° or 180°. However, the four probes at 0°, 60°, 120°, 180° can be adopted to measure the resistance of microbump b_6.

	b_5 (e^- ↑)		$t_{5–6}$	b_6 (e^- ↓)			
Angle (°)	0	180		0	60	120	180
V^+ (node)	3	5	14	11	2	15	12
V^- (node)	6	9	3	14	1	16	13

2.2. Three dimensional finite element models (3D-FEM)

A series of 3D-FEM was also applied to perform an in-depth study of the dimension effect and the current distribution in a microbump. The dimensions of the standard FEM resemble the real microbump sample and the schematic is shown in Fig. 2a. Its tilt view is shown in Fig. 2b, and the Al trace is built to fit the real trace layout of b_6. The material properties used in this FEM is listed in Table 2, and the resistivity of Al is 3.2 µΩ cm [16]. In this study, the resistances at different measured angles on a single microbump were monitored by KBS and the values at the corresponding positions were also obtained in the FEM. In addition, the resistance of a single microbump viewed as an ideal stack of circular disks was also calculated. The three kinds of resistances were then compared to one another. Moreover, a series of microbump resistances which corresponding to 0.4–6.0 µm thick Al trace were obtained to

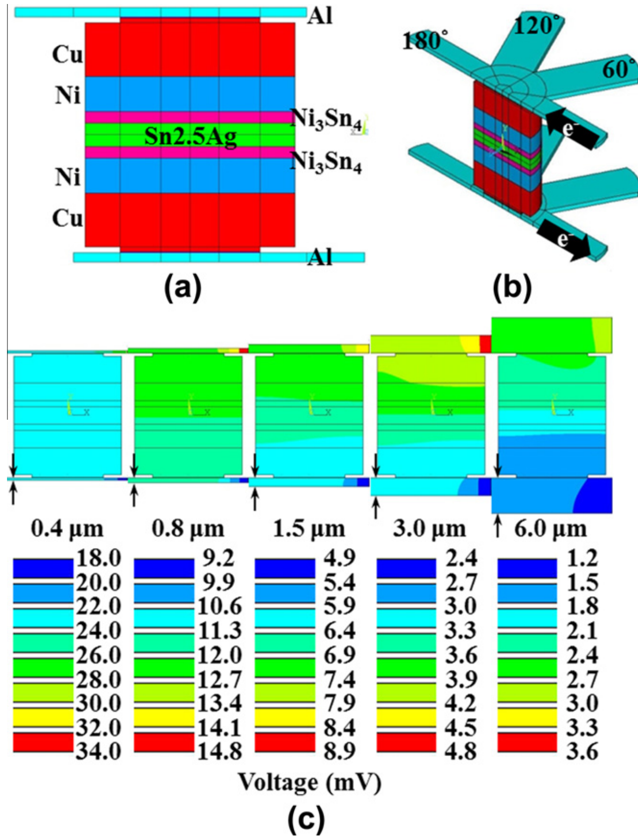

Fig. 2. (a) Cross-sectional view of FEM used in this study. (b) Tilt view of FEM. Four probes in the upper chip can be used to measure the microbump resistance. (c) FEMs with different thicknesses of Al traces.

Table 2
The resistivity values used in FEM.

	Al	Cu	Ni	Ni_3Sn_4	Sn2.5Ag
Resistivity (μΩ -cm)	3.2	1.7	6.8	28.5	12.6

investigate the dimension effect of Al trace. The models with different Al trace thickness are shown in Fig. 2c, and so do the scales of the voltage contour. The scales of the voltage show that the voltage difference between top and bottom is higher in the model with thinner traces.

2.3. Numerical model (NM)

In order to explain the relationship between current distribution in the microbump and the microbump resistance, a simplified numerical model was created in this study. In which the microbump solder joint was viewed as a resistance network, and the joint was divided into n parts vertically. In this numerical model, the current on the left-hand-side is larger than the right-hand-side because of shorter conducting path. Since the current enters from the top left hand corner and exit through the bottom left hand corner, the model can also be used to describe the current crowding phenomenon in microbumps.

The parameters are marked in Fig. 3a, and the corresponding resistance network is shown in Fig. 3b. To simplify the calculation process, the UBM and inter-metallic compound (IMC) were eliminated and the structure was treated as a rectangular solid. The heights of Al trace and solder joint are denoted as H1 and H2. The thickness and the width of the microbump are marked as D

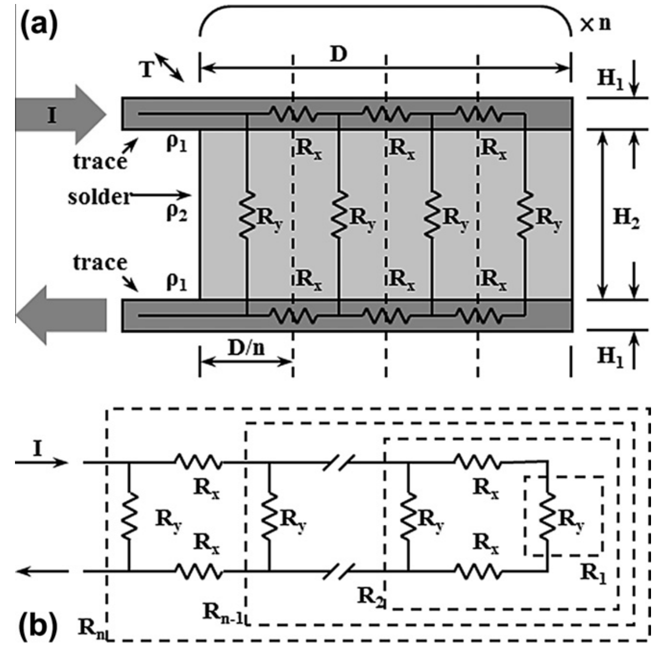

Fig. 3. (a) The schematic plot of numerical model for calculating the resistance of a microbump. (b) The corresponding resistance network diagram.

and T. The resistivity of the traces and solder joint are assigned as ρ_1 and ρ_2. The two-dimensional resistance network is assumed to consist of horizontal and vertical resistances, R_x and R_y, as a parallel circuit. Therefore, the microbump resistance is reachable by calculating the effective resistance of the whole resistance network. The kth effective resistance could be viewed as the parallel connection of the kth R_y and the $(k-1)$th effective resistance and the series of the effective resistance can be written as the following:

$$\begin{aligned} R_1 &= R_y \\ \frac{1}{R_2} &= \frac{1}{R_y} + \frac{1}{2R_x + R_1} \\ &\vdots \\ \frac{1}{R_{n-1}} &= \frac{1}{R_y} + \frac{1}{2R_x + R_{n-2}} \\ \frac{1}{R_n} &= \frac{1}{R_y} + \frac{1}{2R_x + R_{n-1}} \end{aligned} \quad (1)$$

As a result, the relationship between R_n and R_{n-1} could be written in the following form.

$$R_n = \frac{R_y(2R_x + R_{n-1})}{R_y + 2R_x + R_{n-1}} \quad (2)$$

R_n was assumed to be convergent, that is

$$\lim_{n\to\infty} R_{n-1} = \lim_{n\to\infty} R_n \quad (3)$$

With Eq. (3), Eq. (2) is transformed into

$$0 = (\lim_{n\to\infty} R_n)^2 + 2R_x(\lim_{n\to\infty} R_n) - 2R_xR_y \quad (4)$$

Eq. (4) is solved as

$$\lim_{n\to\infty} R_n = R_x + \sqrt{R_x^2 + 2R_xR_y} \quad (5)$$

R_x and R_y are the resistances of a little segment of $\overline{R_x}$ and $\overline{R_y}$. $\overline{R_x}$ is the total horizontal resistance and $\overline{R_y}$ is the total vertical resistance of the solder joint. The relationship therefore becomes

$$R_x = \frac{\overline{R_x}}{n}, R_y = n\overline{R_y} \quad (6)$$

Consequently, Eq. (5) can be written as

$$\lim_{n\to\infty} R_n = \frac{\overline{R_x}}{n} + \sqrt{\left(\frac{\overline{R_x}}{n}\right)^2 + 2\left(\frac{\overline{R_x}}{n}\right)(n\overline{R_y})}$$
$$\lim_{n\to\infty} R_n = \sqrt{2\overline{R_x}\,\overline{R_y}} \tag{7}$$

Finally, a parameter called crowding ratio (C.R.) can be obtained. Crowding ratio is defined as the maximum current density divided by the average value for a specific horizontal layer of solder. It is a very important parameter in electromigration solder joint and represents the non-uniformity of current density. A higher C.R. indicates a higher non-uniform distribution of current density. Therefore, with $n\lim_{n\to\infty} R_n \times I_{total} = R_y \times I_{\max}$ coming from the equal-potential law, the C.R. can be simplifies to

$$\mathrm{C.R} = \frac{J_{\max}}{J_{avg}} = \frac{I_{\max}/\frac{DT}{n}}{I_{total}/DT} = \frac{nI_{\max}}{I_{total}} = \frac{n\lim_{n\to\infty} R_n}{R_y} = \frac{n\lim_{n\to\infty} R_n}{n\overline{R_y}} = \sqrt{2\overline{R_x}/\overline{R_y}} \tag{8}$$

To verify the result, some critical conditions should be taken into consideration, and Eq. (1) should be sensible to the following conditions. First, for the condition of $R_x \to 0$ or $R_y \to \infty$, Eq. (1) becomes invalid. However, these two conditions indicate that current can easily flow horizontally through the Al trace and the pad, but difficult to flow vertically through the portion of solder. Therefore, the current tend to distribute uniformly in the Al trace and the pad before flowing into the solder. As a result, the total effective resistance, $\lim_{n\to\infty} R_n$, approaches $\overline{R_y}$ while R_x becomes smaller or R_y becomes larger. Next, the condition of $R_x \to \infty$ or $R_y \to 0$ means that current crowding is severe because the high trace resistance, $\overline{R_x}$, will force the current quickly flow downward through the solder; the total effective resistance, $\lim_{n\to\infty} R_n$, reaches $\overline{R_y}$ as a result. Furthermore, although the contribution due to the UBM and the IMC part were eliminated in the assumption, it can still be recovered by treating UBM and IMC as rectangular solids to modify $\overline{R_y}$.

3. Results and discussions

3.1. Experimental results obtained from KBS

The microbump resistance measured at 0°, 60°, 120°, and 180° are 74.7, 45.9, 14.6, and 13.7 mΩ respectively, as shown in Table 3 and Fig. 4. However, the resistance is only 13.5 mΩ if a microbump is viewed as an ideal stack of circular metal disks while the current is distributed uniformly in every layer of metal disks. The microbump resistance at 0° monitored by KBS exceeded a 70 mΩ, which is 6 times larger than 13.5 mΩ. If the solder joint is defined to include the Al pads, UBM materials, IMCs, and solder, the microbump resistance obtained from 0° is the closest value to the real microbump resistance because this measurement contains the full voltage drop across the entire solder joint system. The large microbump resistance consequently brings concern because RC delays can significantly change the heat distribution caused by Joule heating. Therefore, understanding the cause of the unexpected large microbump resistance is the first step to improve the electrical performance.

Table 3
The microbump resistances (in milliohm) measured by KBS for microbump b_5, trace t_{5-6}, and microbump b_6.

Sample	b_5 (e^- ↑)		t_{5-6}	b_6 (e^-) (e)			
	0°	180°		0°	60°	120°	180°
No. 1	73.5	14.2	139.8	78.3	47.4	14.5	13.4
No. 2	70.3	18.9	141.2	71.0	44.3	14.7	11.9
No. 3	75.7	13.9	143.7	73.5	–	–	13.6
No. 4	75.1	13.2	142.3	76.0	–	–	15.7
Average	73.7	15.1	141.8	74.7	45.9	14.6	13.7

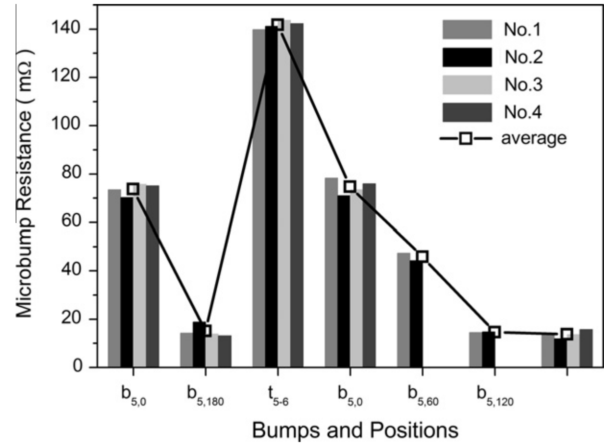

Fig. 4. The measured resistance for bump b_5, trace t_{5-6}, and bump b_6 obtained from KBS.

As the measurement angle is increased, the microbump resistance decreases due to current crowding effect. That is, when the current changes flow-direction, in order to reduce the total resistance in the microbump, a non-uniform current flows through a small area resulting in current crowding effect. (More detail will be discussed in the next section.) Under this kind of circumstance, the high angle measurement position is too far to detect the full voltage drop along the solder joint [15]. Therefore, the microbump resistance significantly decreases with the increasing measurement angle.

3.2. 3D-FEM with different trace thickness

The measured microbump resistances varied with different probe angles and decreased when the angle increases, as shown in the data listed in Table 4. This is due to the reason that at a higher angle, the voltage probe is away from the current crowding region in the Cu UBM. Current crowding is a phenomenon that high current density crowds at the region near the entrance point of electron flow, and it has been the main cause of electromigration failure in solder joints [10,11]. As shown in Fig. 5, this effect induces the non-uniformity of current density and voltage distributions. In addition, although the maximum current density in Sn2.5Ag solder is only 2% higher than the average current density value because of the thick UBM, the current crowding effect is serious in the UBM structure as shown in Fig. 5a and b. Fig. 5c also shows that the majority of voltage drop occurs near the entrance point of electron flow. Because current prefers to flow along the shortest path, the effective conductive area shrinks, and the

Table 4
Microbump resistances (in milliohm) obtained from KBS and FEM with different Al trace thicknesses.

Thickness of t_{5-6} (μm)	t_{5-6}	b_6 (e^-) (e)			
		0°	60°	120°	180°
KBS					
0.8	141.8	74.7	45.9	14.6	13.7
FEM					
0.4	240.0	89.2	84.9	11.4	12.0
0.8	120.0	55.7	52.6	11.6	12.1
1.5	64.0	41.8	40.2	12.3	12.6
3.0	32.0	30.3	29.0	13.3	13.5
6.0	16.0	24.0	23.4	14.7	14.7

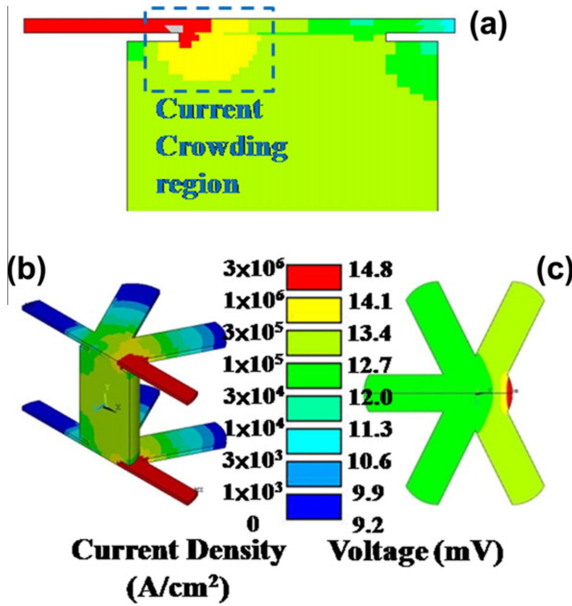

Fig. 5. (a) Cross-sectional view for the simulated current–density distribution in a microbump; the current crowding effect takes place near the entrance point of electron flow. (b) The tilt view of current density distribution in bump b_6. (c) Plan view of voltage distribution in the top Al traces.

voltage dramatically drops at the interface of the Al trace and UBM, causing serious current crowding in the Cu UBM. As a result, the microbump resistance is much higher than the expected value, 13.5 mΩ, calculated by viewing the joint as a simple stack of disks.

There were totally seven locations for resistance measurement monitored simultaneously; but just five results ($t_{5\text{-}6}$ and b_6) are listed in Table 4 because the resistances of b_5 and b_6 show the same trend. In addition, FEM results of different Al trace thickness at different measured angles are also listed in Table 4. From the results, we see that resistances at different angles obtained by FEMs also indicate the same trend as the experimental results by KBS. The resistances at all angles obtained from FEMs decrease dramatically as the Al trace thickened. While the thickness of Al trace is increased from 0.8 to 3.0 μm, the microbump resistances at 0° is decreased from 55.7 to 30.3 mΩ, approaching half of its initial value. The resistance monitored at 0° is specifically discussed, because the resistance at 0° is calculated by the voltage drop along the whole current path in the microbump solder joint.

3.3. Calculated resistance from numerical model

The microbump resistance with different Al trace thicknesses obtained from KBS, FEM, and the numerical model are shown in Table 5 and Fig. 6. The results of the numerical model also matched the trends of KBS and FEM results. Note that the differences between FEM and KBS may be attributed to the disparity of 3D FEM model vs. 2D KBS model. Nevertheless, these results all show

Table 5
Microbump resistances obtained by KBS, FEM, and the numerical model.

Thickness of Al trace (μm)	Microbump resistance (mΩ)		
	KBS	FEM	Numerical model
0.4	–	89.2	84.4
0.8	74.7	55.7	49.7
1.5	–	41.8	31.6
3.0	–	30.3	19.7
6.0	–	24.0	12.6

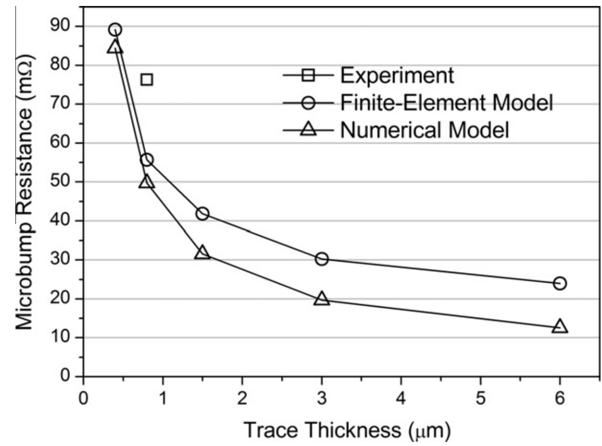

Fig. 6. The microbump resistances obtained by KBS, FEM, and numerical model.

that a microbump with a thicker Al trace has a lower resistance. While the thickness of Al trace is increased from 0.8 to 3.0 μm, the calculated microbump resistance is decreased from 49.7 to 19.7 mΩ. The curves of FEM and the numerical model overlap when the thickness of Al trace is less than 0.8 μm, but split when the Al trace is thicker than 0.8 μm. While the Al trace becomes thicker, the difference between FEM and the numerical model becomes more significant. The reason of the difference is due to the assumption of the existence of serious current crowding at the interface of the traces and the solder joint. When the current crowding is relieved by the thicker trace, the precision of the numerical model is consequently reduced. As mentioned above, the microbump resistance approaches the resistance obtained by viewing the solder joint as a stack of plates in the thick-trace scenario because there is less current crowding effect in the microbump.

4. Conclusions

A KBS was fabricated and the resistances at different measurement angles on a 20.0 μm microbump were precisely monitored. The measured microbump resistance at 0°, 60°, 120°, and 180° are 74.7, 45.9, 14.6, and 13.7 mΩ, respectively. The microbump resistance significantly decreases with increasing measurement angle because of the current crowding effect near the entrance point of the Al trace into the solder. When the resistance is calculated by viewing the microbump as a stack of metal plate, it was only slightly higher than 10 mΩ, much smaller than the resistance obtained from KBS. Nevertheless, the results of KBS, FEM, and NM demonstrate the same trend. The FEM results showed that current is distributed uniformly in the thin solder joint, but current crowding still occurs in the Cu UBM. Regardless of the fact that the maximum current density is only 2% larger than the average value, serious current crowding effect still takes place in the Cu UBM, resulting in the phenomenon of unexpected high microbump resistances. The mismatch between the measurement and the simulation results was partially brought out by the processing control such as the contact area shrinkage and the misalignment. Finally, both 3D-FEMs and numerical model showed that the resistance of a microbump decreases as the thickness of the wiring trace increases. The results implied an effective solution to reduce the high microbump resistance, i.e. thickening the wiring trace. While the thickness of the Al trace is increased from 0.8 to 3.0 μm, the microbump resistances is decreased to half of its original value, resulting from the relieve of current crowding at the interface of the traces and the solder joint.

References

[1] Tu KN. Reliability challenges in 3D IC packaging technology. Microelectron Reliab 2011;51:517–23.
[2] Lin JC, Chiou WC, Yang KF, Chang HB, Lin YC, Liao EB, et al. High density 3D integration using CMOS foundry technologies for 28 nm node and beyond. In: IEEE international electron devices meeting; 2010. p. 2.1.1–4.
[3] Yu A, Lau JH, Ho SW, Kumar A, Hnin WY, Yu DQ, et al. Study of 15 μm pitch solder microbumps for 3D IC integration. In: Electronic components and technology conferences; 2009. p. 6–10.
[4] Tu KN. Recent advances on electromigration in very-large-scale-integration of interconnects. J Appl Phys 2003;94:5451–73.
[5] Chen C, Tong HM, Tu KN. Electromigration and thermomigration in Pb-free flip-chip solder joints. Annu Rev Mater Res 2010;40:531–55.
[6] Shao TL, Chen YH, Chiu SH, Chen C. Electromigration failure mechanisms for SnAg3.5 solder bumps on Ti/Cr–Cu/Cu and Ni(P)/Au metallization pads. J Appl Phys 2004;96:4518–24.
[7] Choi WJ, Yeh ECC, Tu KN. Mean-time-to-failure study of flip chip solder joints on Cu/Ni(V)/Al thin-film under-bump-metallization. J Appl Phys 2003;94:5665–71.
[8] Wright SL, Polastre R, Gan H, Buchwalter LP, Horton R, Andry PS, et al. Characterization of micro-bump C4 interconnects for Si-carrier SOP applications. In: Electronic components and technology conferences; 2006; p. 633–40.
[9] Zhan CJ, Chuang CC, Juang JY, Lu ST, Chang TC. Assembly and reliability characterization of 3D chip stacking with 30 μm pitch lead-free solder micro bump interconnection. In: Electronic components and technology conferences; 2010. p. 1043–9.
[10] Yeh ECC, Choi WJ, Tu KN, Elenius P, Balkan H. Current-crowding-induced electromigration failure in flip chip solder joints. Appl Phys Lett 2002;80:580.
[11] Nah JW, Paik KW, Suh JO, Tu KN. Mechanism of electromigration-induced failure in the 97Pb–3Sn and 37Pb–63Sn composite solder joints. J Appl Phys 2003;94:7560.
[12] Tana YC, Tana CM, Zhangb XW, Chaib TC, Yub DQ. Electromigration performance of through silicon via (TSV) – a modeling approach. Microelectron Reliab 2009;50(9):1336–40.
[13] Liang SW, Chang YW, Chen Chih. Geometrical effect of bump resistance for flip-chip solder joints: finite-element modeling and experimental results. J. Electronic Mater. 2006;35(8):1647–54.
[14] Chang YW, Liang SW, Chen Chih. Study of void formation due to electromigration in flip-chip solder joints using Kelvin bump probes. Appl Phys Lett 2006;89:032103.
[15] Chang YW, Chiang TH, Chen Chih. Effect of void propagation on bump resistance due to electromigration in flip-chip solder joints using Kelvin structure. Appl Phys Lett 2007;91:132113.
[16] Kuan WC, Liang SW, Chen Chih. Effect of bump size on current density and temperature distributions in flip-chip solder joints. Microelectron Reliab 2009;49(5):544–50.